Research Article | Vol. 27, No. 18 / 2 September 2019 / Optics Express 26229
Optics EXPRESS

Slow light engineering in resonant photonic crystal line-defect waveguides

MALIHEH KHATIBI MOGHADDAM AND ROMAIN FLEURY*

Laboratory of Wave Engineering, École Polytechnique Fédérale de Lausanne (EPFL), 1015 Lausanne, Switzerland
romain.fleury@epfl.ch

Abstract: Slow light plays an outstanding role in a wide variety of optical applications, from quantum information to optical processing. While slow optical guiding in photonic crystal waveguides is typically based on Bragg band gaps occurring in non-resonant photonic crystals, here we explore the possibility to leverage the hybridization photonic band gaps of resonant photonic crystals to induce a different form of slow light guiding. We study a line-defect waveguide in a periodic structure composed of high-permittivity resonant dielectric objects and exploit the different guiding mechanisms associated with the hybridization band gap to induce slow light in the resonant phase of the crystal. We demonstrate quantitatively that this method can, in principle, produce high group indices over large bandwidths with potential values of group-index bandwidth products up to 0.67.

1. Introduction

The ability to control the power flow carried by optical pulses, and especially the possibility of obtaining low group velocities is fundamental in the realization of efficient integrated photonic devices [1]. Slow light on a chip has many potential applications including in ultra-compact optical buffers, optical delay lines, and all-optical signal processors [2–6]. Likewise, the interest in slow wave propagation is not limited to optical frequencies and it also finds notable applications at lower frequencies, from the near to far infrared down to the microwave range [7,8]. In optics, non-resonant photonic crystals (PCs) [9] based on Bragg interferences are currently the prevalent solution for slow wave propagation, which is obtained using evanescently coupled cavities or line-defect waveguides [6,10]. These solutions typically rely on light confinement and dispersion engineering with the help of photonic band gaps (PBG), whose physical origin is rooted in Bragg interferences occurring as light is scattered by all the crystal planes [9,11]. A common challenge when it comes to engineering slow light in photonic crystal waveguides (PCWs) is to reduce the group velocity dispersion (GVD), which results in pulse spreading and restricts the bandwidth of slow modes [6,12,13]. This issue is typically addressed through various dispersion engineering methods that aim at creating a constant group index over the largest possible bandwidth, and are generally compared using a figure of merit: the group index-bandwidth product (GBP) [10,13–19].

Photonic crystal band gaps, which originate from interferences in a periodic structure composed of dielectric scatterers, can generally be sorted into two classes, depending on whether the scattering cross-section of the individual scatterers is resonant in the frequency range of interest or not. As an example, a rod-type photonic crystal in the non-resonant phase, supporting traditional Bragg band gaps, can be transformed into a resonant photonic crystal, also known as a locally-resonant metamaterial, by increasing the relative permittivity of the dielectric rods [20–22]. Such all-dielectric resonant photonic crystals offer a variety of optical effects and applications due to the existence of Mie resonances [21,23]. They can be built out of high-index dielectric materials, such as Silicon at visible or near infrared (IR) frequencies, provide a promising low-loss alternative to plasmonic materials, with values of refractive indices up to 5.5

#369816 https://doi.org/10.1364/OE.27.026229
Journal © 2019 Received 18 Jun 2019; revised 5 Aug 2019; accepted 6 Aug 2019; published 30 Aug 2019

Optics EXPRESS

for Germanium in the visible. In the mid infrared (IR), polar crystals can provide indices up to 10, and narrow gap semiconductors such as Te are also used [21,24,25]. The refractive index of Silicon is also known to reach a value of 6.5 in the near UV [23].

Each basic cell in a resonant metamaterial generally includes a locally resonant element which scatters an incident field with a π phase shift above its resonance frequency, resulting in a stopband known as a hybridization bandgap (HBG). The HBG nucleates from the anti-crossing between the light line and the resonator level, a phenomenon similar to level repulsion in a polariton [26–29]. Therefore, light propagation in the resonant phase of this high index crystal is mainly determined by the resonant behavior of the scatterers, rather than the arrangement of the particles (hexagonal or square lattices) [26,30,31]. In some cases, periodicity is not even required, and such resonant metamaterials are often described as homogenized media and studied using effective properties. For instance, one can prove using Lewin's model coupled with Mie scattering theory [32–36] that resonant dielectric particles offer a practical method to obtain negative effective permeability (μ_{eff}) right above their Mie resonance frequency (f_0) [24,32,37]. This negative effective permeability can be interpreted as an HBG. Similar functionalities can be obtained in metamaterials composed of dielectric rods [38], mimicking ferroelectric rods lattices [39], or with polaritonic rods [40] and metallic split-ring resonators [39,41,42]. Since HBG are simply based on local subwavelength resonators, they are relevant for manipulating low-frequency waves in subwavelength acoustics [27,29] and microwaves [26,30,43–46]. Nevertheless, at IR and optical frequencies, dielectric resonators are natural candidates for implementing HBGs considering the fact that metallic resonators are unavailable, as they suffer from increased loss, saturation effects and anisotropic electromagnetic response [24,32]. Therefore, we can wonder whether the different physical origin for wave localization based on HBG in dielectric resonant PCs can represent a new opportunity for inducing slow light with different properties when compared to traditional non-resonant designs.

In this paper, we exploit the HBG and effective properties of a high-index rod-type PC to create a novel class of optical devices for generation of GVD-controlled slow light. First, we recall the scattering behavior of a single dielectric cylindrical particle in the proximity of the Mie resonance frequency and the nucleation of the bandgap due to Fano interferences of a lattice of such Mie resonators. Next, to represent the phase transition in the media and also optimize the width of HBG, we study the effect of the principal parameters of the unit cell. In order to have an optical waveguide, a line-defect structure is created by reducing the rod size in one row of elements, inducing a resonant guided mode inside the bandgap. We qualitatively describe the interaction of different phenomena in shaping the dispersion curve of the guided mode, which interestingly offers a frequency region with nearly constant group velocities. Finally, by dispersion engineering of the guided mode, we propose a set of design parameters for a line-defect waveguide with constant high group-index in a large frequency range, located below the light cone in the middle of the dispersion curve. In particular, we find that dielectric materials with a refractive index of 6, which are for instance readily available in the IR, can be exploited to engineer slow light in a resonant waveguide, with values of GBP potentially higher than state-of-the-art non-resonant photonic crystal waveguides.

2. Result

2.1. Square lattice of high-index rods

When an optical wave hits a high index cylindrical particle (Fig. 1(a)), with a frequency exciting the magnetic Mie resonance, the dielectric particle behaves like a magnetic dipole. The magnetic Mie resonances, which are available at optical frequencies, have circular displacement currents that enhance the magnetic field at the center of the rod. This effect, similar to the one observed in split-ring resonators at sub-THz frequencies, can be exploited to produce negative permeability, in composite optical materials built out of an ensemble of such dielectric Mie resonators, exhibiting

Optics EXPRESS

100% reflection near the resonant frequency [21], due to the nucleation of an HBG. To illustrate this, we consider a square lattice of dielectric circular rods embedded in air (Fig. 1(a)), a configuration frequently studied as a 2D photonic crystal. The TE and TM band diagrams of this 2D lattice considering a relative permittivity of ε'=39 (n = 6.24) and a radius of $r = 0.4a$ are shown in Fig. 1(b), where a is the lattice constant. While the first forbidden band for TM waves is a PBG, the lowest TE bandgap is indeed a HBG that occurs right above the first TE Mie resonance frequency of the rod (f_0), in the normalized frequency range 0.151-0.189 [c/a]. As expected, a 2D structure created by a 8a×8a arrangement of dielectric rods exhibits a strongly suppressed TE transmission in this frequency interval, with S parameters typical of a mirror ($|S_{21}| \approx 0$ and $|S_{11}| \approx 1$, see Fig. 1(c)).

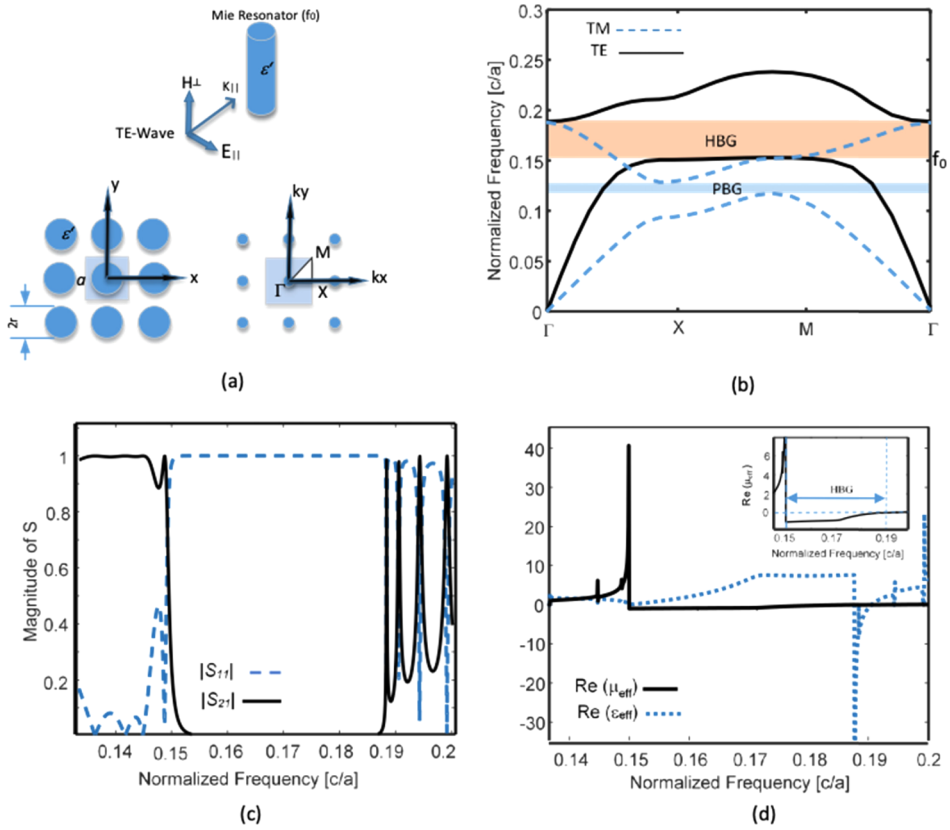

Fig. 1. A simple, all-dielectric, resonant periodic crystal. (a) A dielectric rod with an axis oriented along z-direction ($r = 0.4a$, ε=39) is used as a building block for a square lattice, and the TE modes (H_z, E_x, E_y) are considered. (b) The computed band diagram for the unit cell in ΓXMΓ directions, for both TE and TM modes. (c) Numerically computed S parameters of a two-port structure consist of a 8a×8a lattice of the dielectric rods. (d) The effective permeability of the slab extracted from the S parameters using a standard retrieval method.

Another point of view is to consider this composite of dielectric objects as a continuous bulk medium and characterize it using effective parameters (ε_{eff}, μ_{eff}), as pointed out in Lewin's work [34]. To extract the effective properties of this structure near the HBG, we calculate the real part of the effective relative permeability and permittivity using a known retrieval technique [47,48]. In this method, the complex effective refractive index (N_{eff}) and characteristic impedance (Z_{eff}) are extracted from the numerically computed scattering parameters (S_{21}, S_{11}), which allows

Optics EXPRESS

calculating the constitutive parameters $\mu_{eff} = Z_{eff}\, N_{eff}$ and $\varepsilon_{eff} = N_{eff}/Z_{eff}$. Following the improved algorithm described in [48], here we used the Kramers–Kronig relations to calculate the real part of a complex refractive index from the imaginary part, ensuring the uniqueness of the solution. The result, shown in Fig. 1(d), confirms that the HBG can also be viewed as a single negative medium ($\mu_{eff}<0$), and the polariton tail (right below f_0) as a high index crystal.

Although this structure behaves as a resonant metamaterial near the Mie resonance frequency, it can be driven into the nonresonant photonic crystal phase by continuously changing any of the physical or geometrical parameters. To demonstrate the phase transition of the structure, we investigate the effect of two principal parameters on the configuration of the bandgap for TE polarization, namely the filling ratio and the relative permittivity. Figure 2(a) shows gap maps of TE modes for various values of refractive index (n=$\sqrt{\varepsilon}$), considering the filling ratio fixed at $r/a = 0.25$. The transition from the non-resonant phase to the resonant one occurs at a turning point depicted by the dashed line ($n = 4.4$), where Bragg PBG transforms to HBG. Likewise, the effect of filling ratio (r/a) at a fixed value of the refractive index (ε=39, $n = 6.245$) is shown in the gap map of Fig. 2(b). Although the growth of the filling ratio (r/a) generally expands the HBG, the strong inter-rod near-field interaction for $r/a > 0.45$ is leading to the elimination of Mie resonances and formation of Bragg interferences. Therefore, in the following, we fix the permittivity of the dielectric rods at ε=39 ($n = 6.245$), and the filling ratio to $r/a = 0.4$, which corresponds to good design with relatively large HBG. We stress that such high-index values are currently only available in the IR or for Silicon near 380 nm.

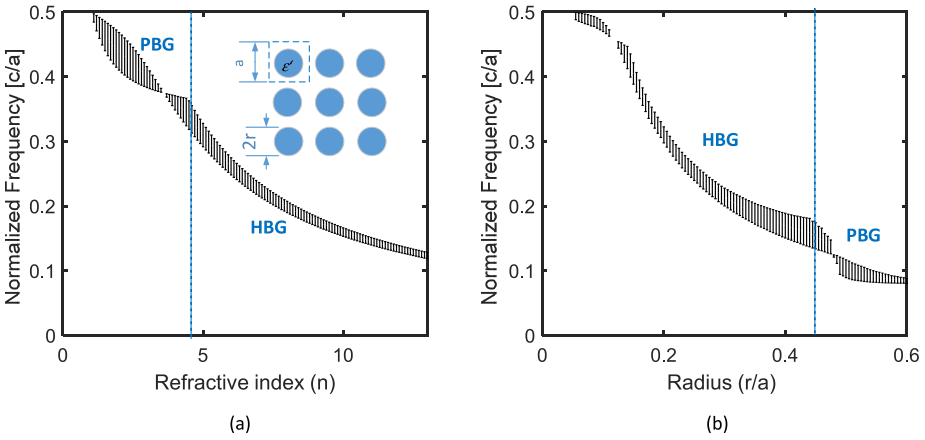

Fig. 2. (a) The gap maps versus refractive index for a fixed value of the dielectric filling ratio, $r = 0.25a$. (b) The gap maps for various values of filling ratio (r/a), for a fixed value of the refractive index n = 6.245 (ε'=39).

2.2. *Line-defect waveguiding in the resonant dielectric crystal*

In the resonant phase, modifying the resonance frequency of particles in one row of the lattice may induce a mode guided along the row by the HBG. This idea is related to prior art demonstrating the use of microwave resonant metamaterials to induce guided waves and slow modes [26,27,43]. Since the HBG nucleates in a frequency range above the individual Mie resonance frequency at f_0=0.15(c/a), inserting a row of reduced-size dielectric rods, implying a slightly higher Mie resonance frequency (f_1), can produce a confined mode traveling in the TE bandgap. Figure 3(a) shows a schematic of such a waveguide, structured using smaller particles (r_1=0.35a), exhibiting a Mie resonance at f_1=0.172 (c/a). This configuration is referred to as configuration A. The dispersion curve of the guided mode of this waveguide, shown in Fig. 3(d) (solid line), indeed

Optics EXPRESS

depicts a guided mode with a cutoff frequency at f_1. Here, the band diagram is computed exclusively for TE modes in the x-direction, considering a supercell with a size of $a\times 20a$ *in xy* plane.

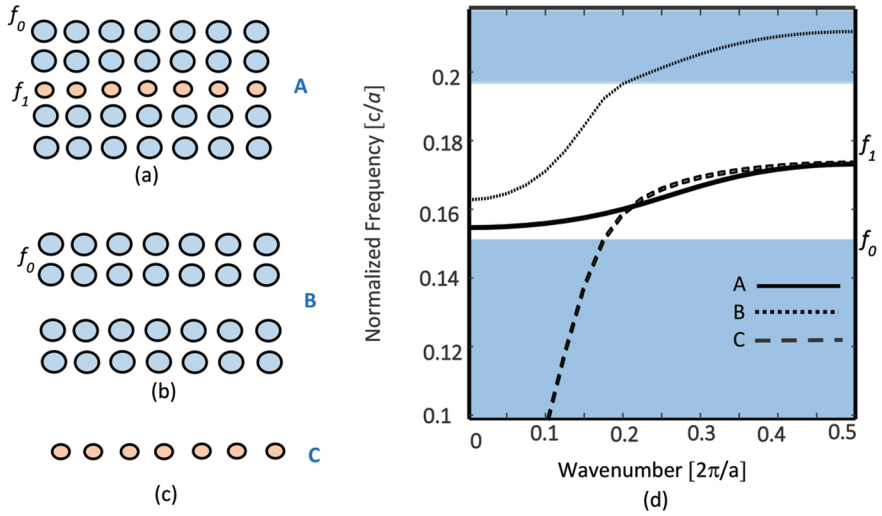

Fig. 3. (a) A line defect waveguide created by reducing the size of rods in one row of lattice considering f_1=0.172 *(c/a)* and f_0=0.15 *(c/a)*. (b) A different line defect waveguide created by removing one row of rods. (c) A linear 1D array of dielectric rods as a cascade of Mie resonators with the resonance frequency of f_1. (d) Dispersion curves of guided modes near the hybridization bandgap frequency for the three different structures labeled by A, B, and C.

The dispersion curve of this localized mode can be described by the interaction of different mechanisms, that are similar to the ones typically found in regular, non-resonant PC line-defect waveguides, albeit activated by different physics. In regular PC waveguides, the dispersion curve of the guided modes can be explained mostly by looking at the interaction of the guiding effects of the surrounding bandgap medium and high-index line defect. Likewise, in this resonant photonic crystal, the dispersion of a mode in the waveguide is shaped by both the HBG effect and the resonant nature of the dielectric line defect. To explain the different phenomena playing a role in the formation of the dispersion curve of waveguide A, we compute the guided modes of two other waveguides, labeled as B and C in Figs. 3(b) and 3(c). Waveguide B, created by removing one row in the lattice, introduces one fast mode, which partly overlaps with the HBG, as shown in Fig. 3(d) (dotted line). This fast mode is guided based on total internal reflection since the crystal behaves as a perfect reflector and reflects back the incoming light into the space left by the line defect.

However, we see that this mode only covers the upper part of the HBG, leaving out a small portion of the bandgap right above the resonant frequency f_0 (near $0.16[c/a]$). In this frequency range, the dispersive nature of the surrounding medium is counter-productive, as it cannot provide the constructive reflection phase needed to form a guided mode. Clearly, this is different from waveguide A, which can support propagation in this lower frequency range, probably due to the presence of the defect line resonators. In order to understand this better, we consider the 1D lattice of dielectric rods with a resonance frequency of f_1, indicated by C in Fig. 3(c). This waveguide is formed by a linear chain built from the defect Mie resonators, and standing in free-space. By coupling via free-space Green's functions, the polarizable particles form a polariton-like dispersion curve (Fig. 3(d)) near f_1. Owing to the high effective permeability (μ_{eff})

Optics EXPRESS

of the chain for $f < f_1$, this 1D crystal can be considered as a high index waveguide, albeit a highly dispersive one [49]. The curves for case A and C are very close to each other near f_1, clearly indicating that high-index guiding is dominant in this range, while the flattening of the band at zero wavenumbers near f_0 indicates guiding dominated by reflections from the surrounding medium. In brief, the dispersion curve of the proposed waveguide A can be described by the hybridization of the fast HBG-based mode in waveguide B and the slow mode near the Mie resonance in waveguide C. The transmission spectra of the different waveguides A, B, and C are shown in Fig. 4(a). The wave propagation in waveguides A and B is shown in Fig. 4(b) and 4(c), respectively. The field profiles are computed using the 2D finite difference time domain (FDTD) method for a narrow band continuous wave pulse with a central frequency of 0.165[c/a]. They demonstrate clearly a localized spectrum for waveguide A inside the band gap, right between f_0 and f_1. Note that these two frequencies correspond to the magnetic Mie resonance frequencies of the gap and defect rods, which can be tuned to vary both the guided mode bandwidth and group velocity, or equivalently, its GBP. We therefore conclude that such a guiding method provides interesting degrees of freedom to control both the bandwidth and group-index of light.

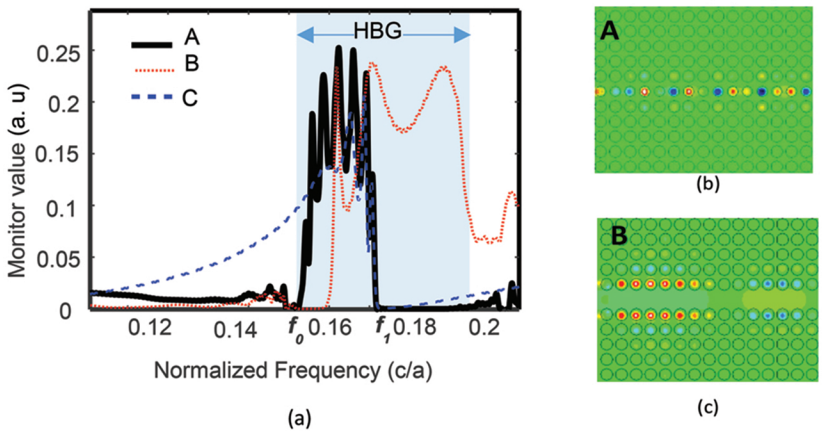

Fig. 4. (a) The typical transmission spectra for the three waveguiding structures shown by A, B, and C, computed by 2D FDTD. (b) Propagation of a narrow band continuous-wave pulse with a central frequency of f_c=0.165[c/a] in the proposed waveguide A. (c) Fast wave propagation in the line-defect waveguide created by removing one row of rods (waveguide B)

2.3. *Dispersion-controlled slow light*

In this section, we discuss the possibility to induce dispersion-controlled slow light in the proposed line-defect waveguide. Typically, slow light suffers from high group velocity dispersion (GVD), which cause pulse broadening and practically limits the usable bandwidth available under a constant group index (n_g=c/v_g), where c is speed of light and v_g is the group velocity [6,12]. The GVD parameter of $\beta_2 = \partial/\partial\omega(1/v_g)$, which shows the variation of group index versus angular frequency (ω), is commonly used for evaluation of optical devices. In all slow light devices, an inherent tradeoff must be considered, where higher group index values result in smaller bandwidth. Thus, slow light waveguides are generally evaluated using a combined figure of merit, the group index-bandwidth product $GBP = \widetilde{n_g}(\Delta\omega/\omega_0)$, ω here $\widetilde{n_g}$ is the average group-index, ω_0 is the central angular frequency, and $\Delta\omega$ is defined as the angular frequency range in which the variation of n_g with respect to its mean value is less than 10%.

Optics EXPRESS

In PCWs, the GVD problem is often mitigated using dispersion engineering methods that allow control over the shape of the dispersion curve. These methods aim at extending flat-band frequency regions, where the slope of the dispersion curve is small and as constant as possible. Here, we use a similar approach to control the shape of the dispersion curve and realize flat-band slow light, leveraging the unique degrees of freedom offered in the dispersions of both the band gap medium and the guiding line-defect.

As can be seen in Fig. 3(d), the dispersion curve of waveguide A, considering r_1=0.35a, offers a low group velocity region near the band edge (f_1). However, slow light in this frequency region suffers from strong GVD, which restricts the operating bandwidth. Yet, in a frequency region located in the middle of guiding band, the slope of the dispersion curve is almost constant. This is an interesting feature that one can try to leverage to construct a slow light waveguide with relatively high group index and higher bandwidth. Indeed, by modification of the size or permittivity of the rods inside the waveguide, we can not only alter the Mie resonance frequency of the particles but also control the shape of the dispersion curve. Figure 5(a) indicates the dispersion curve of guided modes for different values of r_1 ($0.32a < r_1 < 0.38a$). As the size of the rod grows, f_1 shifts up and the interaction of the HBG guiding and high-index dispersive guiding builds up a lower group-index mode with a wider bandwidth. This is evidenced in Fig. 5(b) and 5(c), which directly plot the group index (n_g) and GVD (β_2) of these waveguides as a function of frequency. Smaller rods result in lower group-indices, yet over larger flat band. Due to the high refractive index of the dielectric particles, the flat band region of the guided modes are located in the low normalized frequency region, well below the light line. Thus the bandwidth of the slow modes are not mitigated by considering the leaky modes above the light lines. We have also checked that considering a 3D structure with finite-sized cylinders does not change these findings, providing one properly rescales the cylinder radius to compensate for a finite cylinder height. Figure 6(a)–6(b) summarizes the group index and the fractional bandwidth of the flat band slow modes versus the values of radii (r_1). This data is summarized into a single metric, the GBP, in Fig. 6(c). In addition, one can perform slight tuning of the value of the permittivity of the dielectric rods in the line defect waveguide in order to tune the localization of the localized mode inside the HBG. For cylindrical elements with $25 < \varepsilon_1 < 36$, considering r_1=0.4a, the computed values of group indices, fractional bandwidths, and GBP are presented in Fig. 6(d)–6(f).

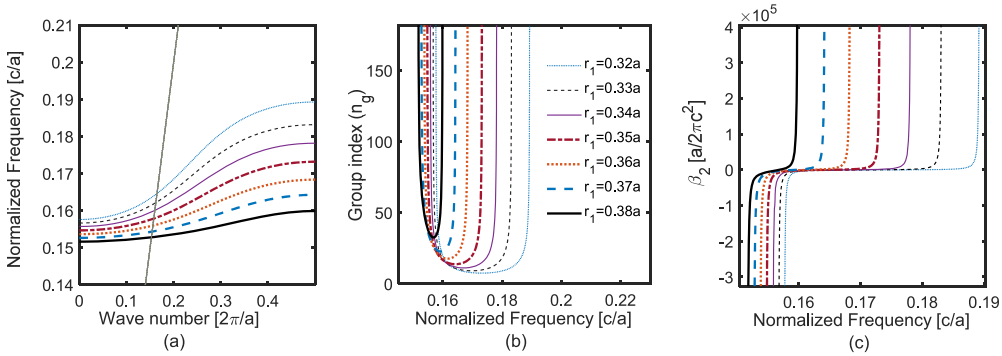

Fig. 5. (a) Dispersion curve of line-defect modes inside the band gap and. The gray thin line shows the light line. (b) The group index versus frequency for $0.32a < r_1 < 0.38a$. (c) GVD versus frequency. Note that the near-zero GVD region correspond to the middle of the band, which falls below the light line.

As demonstrated in Fig. 6(a)–6(f), by enhancing the filling ratio (r_1/a), permittivity (ε), or equivalently decreasing the resonance frequency of the defects particles, the bandwidth of the guided mode is reduced, but the group velocity is increased. Despite the large bandwidth

Optics EXPRESS

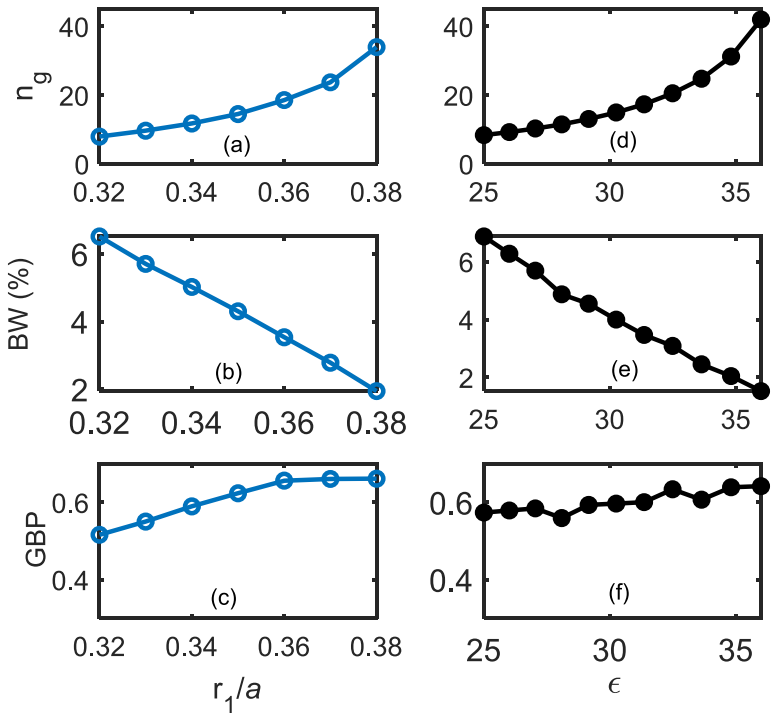

Fig. 6. The group index (a, d), bandwidth (b, e), and the GBP (c, f) of the resonant photonic crystal line-defect waveguide for various values of ε_1 and r_1

obtained for smaller and low-index rods, e.g. r_1=0.32a (ε_1=39) and ε_1=25 (r_1=r = 0.4a), the highest amount of GBP is achieved for waveguides constructed using rods with larger size and permittivity. Consequently, using the new approach of constructing a line-defect waveguide in a resonant photonic crystal, we demonstrate that a high value of GBP = 0.67, with n_g=34 and fractional bandwidth of 2%, can be obtained for r_1 = 0.38a (ε_1=39). This high value of GBP shows a significant improvement in comparison with 2D dispersion engineered slow light waveguides in the conventional non-resonant photonic crystal, which are associated with GBP typically in the range of 0.1-0.4.

3. Summary

In summary, we proposed a novel approach leveraging the inherent dispersion of locally-resonant photonic crystals, also known as locally-resonant crystalline metamaterials, as a new degree of freedom to induce a new generation of slow-light waveguides with unusual dispersive properties. By combining dispersive high-index guiding and guiding based on dispersive total internal reflection, we demonstrated numerically a novel form of dispersive optical waveguide supporting light transport with small group velocity. We also showed how the interaction of different phenomena, including Fano interferences of Mie resonators, hybridization band gap, and abnormal dispersive effective permeability near the Mie resonance frequency of the particles, shape the dispersion curve of this waveguide and allow for engineering its group bandwidth product. Although narrow band ultra-slow light with high group velocity dispersion can be obtained near the band edge, a potentially more interesting frequency region with nearly constant group index was identified, located in the middle of the dispersion curve. By adjusting the size and permittivity of defect rods and controlling the shape of the dispersion curve, flat-band slow

Optics EXPRESS

light was obtained with a GBP of 0.67. Note that our design involves an index of refraction of 6, which is readily available in the IR, however we believe that a design in the visible is also possible with Germanium, whose index can go up to 5.5, by adjusting the geometrical parameters. We believe that this method has the potential to provide GBP values larger than the ones obtained with dispersion-engineered slow light based on photonic crystals in the non-resonant phase.

Funding

Hassler Foundation.

Acknowledgments

M. K. M. acknowledges funding from the Hasler Foundation. The authors would like to thank Dr. Bakhtiyar Orazbayev and Dr. Nadège Kaina for useful discussions about the physics of locally resonant metamaterials, subwavelength waveguiding, and retrieval method of effective parameters.

References

1. T. F. Krauss, "Why do we need slow light?" Nat. Photonics **2**(8), 448–450 (2008).
2. V. R. Almeida, C. A. Barrios, R. R. Panepucci, and M. Lipson, "All-optical control of light on a silicon chip," Nature **431**(7012), 1081–1084 (2004).
3. A. Shinya, E. Kuramochi, H. Taniyama, T. Tanabe, and M. Notomi, "Trapping and delaying photons for one nanosecond in an ultrasmall high-Q photonic-crystal nanocavity," Nat. Photonics **1**(1), 49–52 (2007).
4. F. Xia, L. Sekaric, and Y. Vlasov, "Ultracompact optical buffers on a silicon chip," Nat. Photonics **1**(1), 65–71 (2007).
5. M. D. Lukin and A. Imamoğlu, "Controlling photons using electromagnetically induced transparency," Nature **413**(6853), 273–276 (2001).
6. T. Baba, "Slow light in photonic crystals," Nat. Photonics **2**(8), 465–473 (2008).
7. S. Savo, B. D. F. Casse, W. Lu, and S. Sridhar, "Observation of slow-light in a metamaterials waveguide at microwave frequencies," Appl. Phys. Lett. **98**(17), 171907 (2011).
8. E. Di Gennaro, P. V. Parimi, W. T. Lu, S. Sridhar, J. S. Derov, and B. Turchinetz, "Slow microwaves in left-handed materials," Phys. Rev. B **72**(3), 033110 (2005).
9. J. J. D. Joannopoulos, S. Johnson, J. N. J. Winn, and R. R. D. Meade, *Photonic Crystals: Molding the Flow of Light* (2008).
10. A. Badolato, R. Houdré, M. Minkov, R. W. Boyd, M. S. Mohamed, B. Gao, Y. Lai, and V. Savona, "Ultra-wide-band structural slow light," Sci. Rep. **8**(1), 1–5 (2018).
11. S. G. Johnson, S. Fan, P. R. Villeneuve, J. D. Joannopoulos, and L. A. Kolodziejski, "Guided modes in photonic crystal slabs," Phys. Rev. B **60**(8), 5751–5758 (1999).
12. J. Goor, N. Asger, P. Review, B. C. Matter, D. Version, and C. Matter, "Limits of slow light in photonic crystals," Phys. Rev. B **78**(15), 153101 (2008).
13. L. O'Faolain, D. M. Beggs, T. P. White, A. Melloni, T. F. Krauss, and S. A. Schulz, "Dispersion engineered slow light in photonic crystals: a comparison," J. Opt. **12**(10), 104004 (2010).
14. M. Notomi, K. Yamada, A. Shinya, J. Takahashi, C. Takahashi, and I. Yokohama, "Extremely large group-velocity dispersion of line-defect waveguides in photonic crystal slabs," Phys. Rev. Lett. **87**(25), 253902 (2001).
15. M. Khatibi Moghaddam, A. R. Attari, and M. M. Mirsalehi, "High coupling efficiency to a low dispersion slow light-supporting photonic crystal waveguide," J. Eur. Opt. Soc. **8**, 13066 (2013).
16. N. Matsuda, E. Kuramochi, H. Takesue, and M. Notomi, "Dispersion and light transport characteristics of large-scale photonic-crystal coupled nanocavity arrays," Opt. Lett. **39**(8), 2290–2293 (2014).
17. R. Hao, E. Cassan, X. Le Roux, D. Gao, V. Do Khanh, L. Vivien, D. Marris-Morini, and X. Zhang, "Improvement of delay-bandwidth product in photonic crystal slow-light waveguides," Opt. Express **18**(16), 16309 (2010).
18. R. Hao, E. Cassan, H. Kurt, X. Le Roux, D. Marris-Morini, L. Vivien, H. Wu, Z. Zhou, and X. Zhang, "Novel slow light waveguide with controllable delay-bandwidth product and utra-low dispersion," Opt. Express **18**(6), 5942 (2010).
19. S. A. Schulz, L. O'Faolain, D. M. Beggs, T. P. White, A. Melloni, and T. F. Krauss, "Dispersion engineered slow light in photonic crystals: A comparison," J. Opt. **12**(10), 104004 (2010).
20. I. Staude and J. Schilling, "Metamaterial-inspired silicon nanophotonics," Nat. Photonics **11**(5), 274–284 (2017).
21. S. Jahani and Z. Jacob, "All-dielectric metamaterials," Nat. Nanotechnol. **11**(1), 23–36 (2016).
22. M. V. Rybin, D. S. Filonov, K. B. Samusev, P. A. Belov, Y. S. Kivshar, and M. F. Limonov, "Phase diagram for the transition from photonic crystals to dielectric metamaterials," Nat. Commun. **6**(1), 10102 (2015).

Optics EXPRESS

23. D. G. Baranov, D. A. Zuev, S. I. Lepeshov, O. V. Kotov, A. E. Krasnok, A. B. Evlyukhin, and B. N. Chichkov, "All-dielectric nanophotonics: the quest for better materials and fabrication techniques," Nanophotonics **4**(7), 814–825 (2017).
24. X. Liu, Q. Zhao, C. Lan, and J. Zhou, "Isotropic Mie resonance-based metamaterial perfect absorber," Appl. Phys. Lett. **103**(3), 031910 (2013).
25. C. L. Holloway, E. F. Kuester, J. Baker-Jarvis, and P. Kabos, "A Double Negative (DNG) Composite Medium Composed of Magnetodielectric Spherical Particles Embedded in a Matrix," IEEE Trans. Antennas Propag. **51**(10), 2596–2603 (2003).
26. F. Lemoult, N. Kaina, M. Fink, and G. Lerosey, "Wave propagation control at the deep subwavelength scale in metamaterials," Nat. Phys. **9**(1), 55–60 (2013).
27. S. Yves, R. Fleury, F. Lemoult, M. Fink, and G. Lerosey, "Topological acoustic polaritons: Robust sound manipulation at the subwavelength scale," New J. Phys. **19**(7), 075003 (2017).
28. N. Kaina, F. Lemoult, M. Fink, and G. Lerosey, "Negative refractive index and acoustic superlens from multiple scattering in single negative metamaterials," Nature **525**(7567), 77–81 (2015).
29. Z. Liu, X. Zhang, Y. Mao, and Y. Y. Zhu, "Locally Resonant Sonic Materials," Science **289**(5485), 1734–1736 (2000).
30. N. Kaina, F. Lemoult, M. Fink, and G. Lerosey, "Ultra small mode volume defect cavities in spatially ordered and disordered metamaterials," Appl. Phys. Lett. **102**(14), 144104 (2013).
31. E. E. Maslova, M. F. Limonov, and M. V. Rybin, "Transition between a Photonic Crystal and a Metamaterial with Electric Response in Dielectric Structures," JETP Lett. **109**(5), 340–344 (2019).
32. Q. Zhao, J. Zhou, F. Zhang, and D. Lippens, "Mie resonance-based dielectric metamaterials," Mater. Today **12**(12), 60–69 (2009).
33. Q. Zhao, B. Du, L. Kang, H. Zhao, Q. Xie, B. Li, X. Zhang, J. Zhou, L. Li, and Y. Meng, "Tunable negative permeability in an isotropic dielectric composite," Appl. Phys. Lett. **92**(5), 051106 (2008).
34. L. Lewin, "The electrical constants of a material loaded with spherical particles," J. Inst. Electr. Eng., Part 3 **94**(27), 65–68 (1947).
35. C. L. Holloway, E. F. Kuester, J. Baker-Jarvis, and P. Kabos, "A Double Negative (DNG) Composite Medium Composed of Magnetodielectric Spherical Particles Embedded in a Matrix," IEEE Trans. Antennas Propag. **51**(10), 2596–2603 (2003).
36. D. Felbacq and G. Bouchitté, "Negative refraction in periodic and random photonic crystals," New J. Phys. **7**, 159 (2005).
37. B. A. Slovick, Z. G. Yu, and S. Krishnamurthy, "Generalized effective-medium theory for metamaterials," Phys. Rev. B **89**(15), 155118 (2014).
38. K. Vynck, D. Felbacq, E. Centeno, A. I. Căbuz, D. Cassagne, and B. Guizal, "All-dielectric rod-type metamaterials at optical frequencies," Phys. Rev. Lett. **102**(13), 133901 (2009).
39. S. O'Brien and J. B. Pendry, "Magnetic activity at infrared frequencies in structured metallic photonic crystals," J. Phys.: Condens. Matter **14**(25), 3076383–6394 (2002).
40. K. C. Huang, M. L. Povinelli, and J. D. Joannopoulos, "Negative effective permeability in polaritonic photonic crystals," Appl. Phys. Lett. **85**(4), 543–545 (2004).
41. W. J. Padilla, D. N. Basov, and D. R. Smith, "Negative refractive index metamaterials," Mater. Today **9**(7-8), 28–35 (2006).
42. E. Ozbay, K. Guven, and K. Aydin, "Metamaterials with negative permeability and negative refractive index: Experiments and simulations," J. Opt. A: Pure Appl. Opt. **9**(9), S301–S307 (2007).
43. N. Kaina, A. Causier, Y. Bourlier, M. Fink, T. Berthelot, and G. Lerosey, "Slow waves in locally resonant metamaterials line defect waveguides," Sci. Rep. **7**(1), 15105 (2017).
44. S. Yves, R. Fleury, T. Berthelot, M. Fink, F. Lemoult, and G. Lerosey, "Crystalline metamaterials for topological properties at subwavelength scales," Nat. Commun. **8**(1), 16023 (2017).
45. A. A. Maznev and V. E. Gusev, "Waveguiding by a locally resonant metasurface," Phys. Rev. B **92**(11), 115422 (2015).
46. B. Orazbayev, N. Kaina, and R. Fleury, "Chiral waveguides for robust waveguiding at the deep subwavelength scale," Phys. Rev. Appl. **10**(5), 054069 (2018).
47. X. Chen, T. M. Grzegorczyk, B. I. Wu, J. Pacheco, and J. A. Kong, "Robust method to retrieve the constitutive effective parameters of metamaterials," Phys. Rev. E **70**(1), 016608 (2004).
48. Z. Szabó, G. H. Park, R. Hedge, and E. P. Li, "A unique extraction of metamaterial parameters based on Kramers-Kronig relationship," IEEE Trans. Microwave Theory Tech. **58**(10), 2646–2653 (2010).
49. A. Alù and N. Engheta, "Theory of linear chains of metamaterial/plasmonic particles as subdiffraction optical nanotransmission lines," Phys. Rev. B **74**(20), 205436 (2006).